The MICADO first light imager for the ELT: preliminary design of the MICADO Calibration Assembly

Rodeghiero, G., Pott, J.-U., Münch, N., Rohloff, R.-R., Grözinger, U., et al.

G. Rodeghiero, J.-U. Pott, N. Münch, R.-R. Rohloff, U. Grözinger, E. Biancalani, M. Sawczuck, M. Häberle, J. Moreno-Ventas, S. Schäfer, U. Seemann, V. Naranjo, S. Barboza, F. Müller, R. Hofferbert, J. Ramos, L. Mohr, M. C. Cárdenas Vázquez, P. Bizenberger, C. Pernechele, M. Ebert, M. Fabricius, "The MICADO first light imager for the ELT: preliminary design of the MICADO Calibration Assembly," Proc. SPIE 10702, Ground-based and Airborne Instrumentation for Astronomy VII, 107028U (11 July 2018); doi: 10.1117/12.2311721

SPIE.

Event: SPIE Astronomical Telescopes + Instrumentation, 2018, Austin, Texas, United States

The MICADO first light imager for the ELT: preliminary design of the MICADO Calibration Assembly

G. Rodeghiero[a*], J.-U. Pott[a], N. Münch[a], R.-R. Rohloff[a], U. Grözinger[a], E. Biancalani[a], M. Sawczuck[a], M. Häberle[a], J. Moreno-Ventas[a], S. Schäfer[b], U. Seemann[b], V. Naranjo[a], S. Barboza[a], F. Müller[a], R. Hofferbert[a], J. Ramos[a], L. Mohr[a], M. C. Cárdenas Vázquez[a], P., Bizenberger[a], C. Pernechele[c], M. Ebert[a], M. Fabricius[d]

[a] Max Planck Institute for Astronomy - Königstuhl 17, 69117 Heidelberg, Germany
[b] Georg August Universität Göttingen, Institute for Astrophysics, Friedrich-Hund-Platz 1, 37077 Göttingen, Germany
[c] INAF OAPD, Vicolo Osservatorio 5, 35122 Padova, Italy
[d] Max Planck Institute for extraterrestrial Physics, 85748 Garching, Germany

ABSTRACT

The paper describes the preliminary design of the MICADO calibration assembly. MICADO, the Multi-AO Imaging CAmera for Deep Observations, is targeted to be one of the first light instruments of the Extremely Large Telescope (ELT) and it will embrace imaging, spectroscopic and astrometric capabilities including their calibration. The astrometric requirements are particularly ambitious aiming for ~ 50 μas differential precision within and between single epochs. The MICADO Calibration Assembly (MCA) shall deliver flat-field, wavelength and astrometric calibration and it will support the instrument alignment to the Single-Conjugate Adaptive Optics wavefront sensor. After a complete overview of the MCA subsystems, their functionalities, design and status, we will concentrate on the ongoing prototype testing of the most challenging components. Particular emphasis is put on the development and test of the Warm Astrometric Mask (WAM) for the calibration of the optical distortions within MICADO and MAORY, the multi-conjugate AO module.

Calibration unit, astrometry, distortion, spectroscopy, near infrared imaging.

1. INTRODUCTION

This work presents the preliminary design of the MICADO Calibration Assembly (MCA) on its way to the Preliminary Design Review (PDR) expected at the end of 2018. MICADO will be one of the first light instruments of the ELT expected to start operations by the end of the next decade and it will provide near infrared (0.8 - 2.4 μm) imaging and spectroscopy, with a target relative astrometric precision of ~ 50 μas over the full Field of View (FoV) of 53". MICADO will be assisted both by a Single-Conjugate Adaptive Optics (SCAO) system, that will provide a corrected FoV = 19" and by a Multi-Conjugate Adaptive Optics (MCAO) system with the Multi-conjugate Adaptive Optics RelaY (MAORY) that will enable diffraction limited observations over the whole instrument FoV (53") by means of two post-focal deformable mirrors conjugated at about ~5 and ~12 km height [1]. During the acceptance, integration and verification

* rodeghiero@mpia.de; phone (+49/0) 6221528-258

Ground-based and Airborne Instrumentation for Astronomy VII, edited by Christopher J. Evans, Luc Simard, Hideki Takami, Proc. of SPIE Vol. 10702, 107028U · © 2018 SPIE · CCC code: 0277-786X/18/$18 · doi: 10.1117/12.2311721

phase MICADO will operate in the so-called 'standalone' mode without the MCAO correction relying only on SCAO and relying on a smaller relay optics. This mode will be eventually used also for the early instrument operations in case MAORY and MICADO will have a relative delay. Being MICADO the first light instrument of ELT, it will offer a wide range of observing modes [2] spanning from wide field diffraction limited imaging with a special devotion to astrometry, single object echelle spectroscopy at R ~ 14,000, high contrast imaging with coronagraphy. In this perspective, MICADO will be the first instrument to combine the huge collecting area of ELT (~ 1,200 m^2), diffraction limited capabilities and superb astrometric accuracy over ~ 1 arcmin FoV. With MICADO, the theoretical astrometric precision $\sigma \sim FWHM/SNR$ [3] will improve by a factor ~ 5 with respect to the current generation of instruments at the 8 m class telescopes, leading to achieve an astrometric precision of ~ 50 μas within a single epoch. MICADO is placed at one of the Nasmyth platforms in a gravity invariant configuration to ensure the maximum opto-mechanical stability. The instrument will provide two imaging modes: full field, 53" FoV with 4.5 mas pixel scale, and zoom mode with 19" FoV with 1.5 mas pixel scale; the latter is characterized by an optical path with no moving parts to provide the highest astrometric stability. Achieving these ambitious performances requires a non-trivial calibration effort that goes beyond the calibration of the instrument alone and embraces also the systematics coming from the telescope and the fore optics (standalone relay optics resp. MAORY). In this paper we present the preliminary design of the MCA (Chapter 2), discuss the first results of the prototype testing (Chapter 3), and present a more general overview of the challenges, potentialities and limitations of the astrometric calibration (Chapter 4).

2. THE MICADO CALIBRATION ASSEMBLY

The MCA consists of 4 units as shown in Figure 1:

- Flat-field and wavelength Calibration Unit (FCU)
- Astrometric Calibration Unit (ACU)
- Movable source Calibration Unit (MCU)
- Deployable Mirror Unit (DMU)

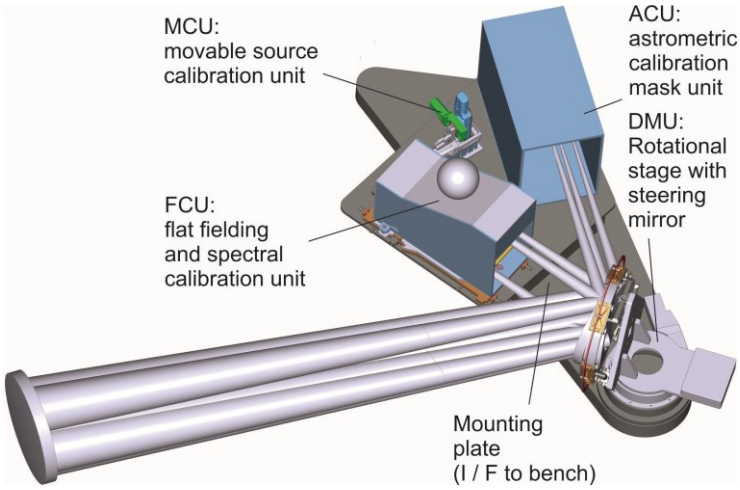

Figure 1: MCA overview: three calibration units to allow for flat-field, wavelength and astrometric calibrations and a movable source for calibrations of the SCAO WFS and alignment purposes. The light from the MCA is conveyed to the instrument through

a deployable mirror that is moved into the beam by a rotation stage during the calibration run and moved out of the beam during observations.

2.1 MCA deployment mechanism

At the current phase of the MICADO project (PDR) two instrument modes coexist and are developed in parallel:

- MCA standalone Relay Optics (RO) mode, MICADO alone assisted only by SCAO. In this mode, for Assembly Integration and Verification (AIV) and pre-MAORY phase, MICADO is placed at the focus of standalone RO that brings the ELT focal plane (FP) to an accessible position for the instrument (Fig.2 left). The MCA is placed in proximity of the ELT FP and its functionalities are delivered to the instrument by the DMU.

- MCA MAORY mode, MICADO assisted by MCAO. The ELT FP is relayed by MAORY to MICADO with the same f/# and the wavefront is corrected for the atmospheric and telescope aberrations. In this configuration the MCA is placed on the MAORY bench and MICADO is mounted under the MAORY bench. (Fig.2 right).

In both modes, the light from the MCA units is coupled to MICADO with an auxiliary deployable mirror (DMU) that is deployed during the calibration run and it redirects the light into the standalone RO or MAORY.

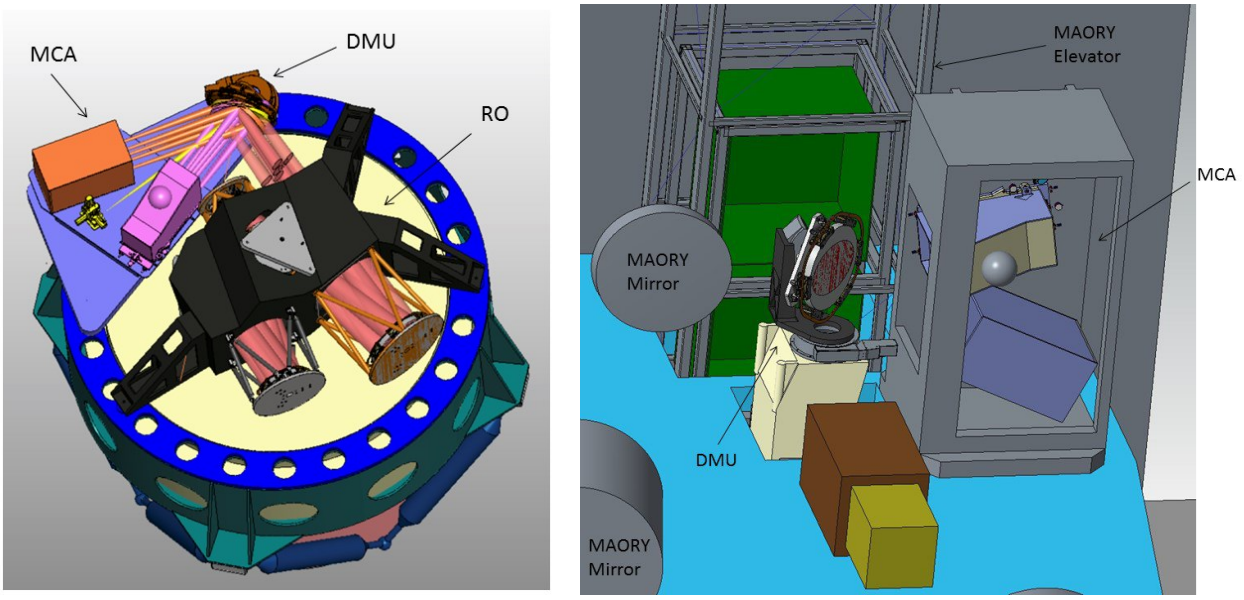

Figure 2, **Left:** MCA on the standalone RO bench with the deployable mirror collecting the light from the three calibration units, drawing by KTO GmbH that is responsible for the DMU design until PDR. The DMU is rotated out of the beam during astronomical observations. **Right:** the MCA on the MAORY bench is installed close to the elevator of the MAORY calibration unit assembly and it is deployed also by a deployable mirror solution. The DMU is brought to the calibration position from below the MAORY bench with a small elevator.

Another possible solution, at the moment kept as backup plan, is unbundling the MCA subunits and place them into the MAORY elevator together with the MAORY calibration unit and the calibration unit for the second instrument assisted by MAORY. The MAORY elevator is deployed directly at the ELT focal plane and parked below the MAORY bench during observations. The baseline for PDR is a separate deployment mechanism (DMU) placed at the MAORY bench,

that leads to separate mechanical, electrical and software interfaces between MAORY and MICADO calibration units and to a smaller MAORY elevator. In case the MCA subunits are placed in the MAORY elevator the DMU is not needed. More details about the MAORY preliminary design can be found in [4].

2.2 Flat-field and wavelength calibration unit - FCU

The FCU provides a flat-field calibration through a continuum light source (tungsten bulb lamp) to the MICADO instrument for the calibration of the detector response in terms of quantum efficiency and its pixel to pixel variations, mapping of hot/dead pixels and vignetting factors. The FCU shall also provide multiple light sources with an emission line spectrum to provide a wavelength solution of the instrument spectrograph. The light from the sources is collected in the FCU and diffused by means of an Integration Sphere (IS) and a Spectralon panel towards the MAORY-MICADO optics. The FCU is close to the ELT FP and its light is fed to the standalone RO / the MAORY optics by means of the DMU. A baffle limits the stray light production while the rays with the f/# matching that of the standalone RO / the MAORY optics propagate into the system and are injected into MICADO. The calibration takes place periodically at every observation run during day-time for the flat-field and the wavelength calibration, and occasionally during night-time for the latter. Many astronomical instruments currently used on the 8 m class telescopes [5], [6], [7], [8] deploy (with a pick-off mirror) or reimage directly the exit port of the IS at the entrance focal plane of the instrument; this is not possible for MICADO having an entrance focal plane of ~ 200 mm x 200 mm that would require an impractically large IS. The issue is overcome by using a relatively small IS (~ 280 mm) coupled with a large Spectralon panel (highly diffusing Lambertian material) placed at the standalone RO/ the MAORY entrance focal plane and deployed with the DMU during the calibration run. The IS is placed off-axis with respect to the Spectralon panel to avoid vignetting of the field and the light is conveyed to the panel by a flat mirror as shown in Figure 3.

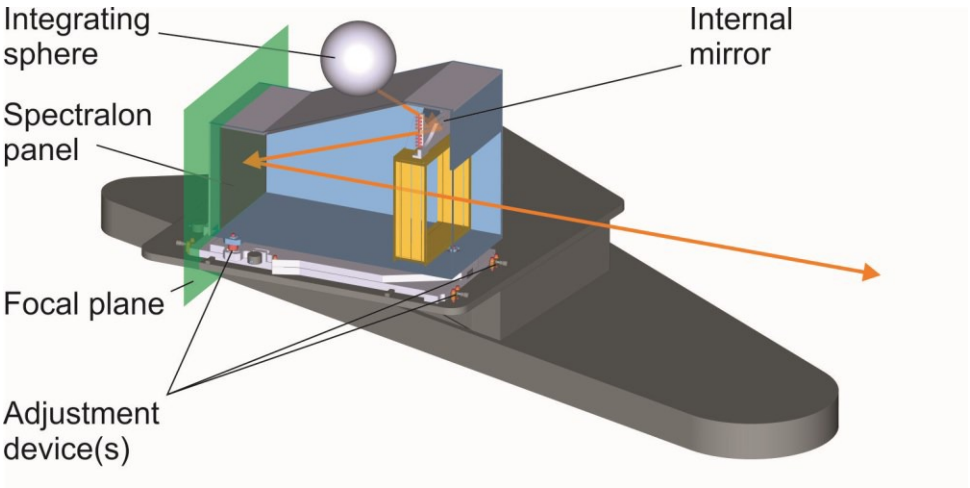

Figure 3: View of the FCU used for the flat-field and wavelength calibration of MICADO.

The Angle of Incidence (AoI) of the rays hitting the Spectralon panel shall not exceed 40 degrees to ensure a Lambertian diffusion of the flat-field light [9] (see Fig. 4). A shutter (not shown) is used to block the light flux from the bulb lamp during the warming up phase. A NIR photodiode (not shown) is placed in the proximity of the bulb lamp to provide health feedback to the instrument control software and to monitor the flux stability and the performance degradation of the lamp.

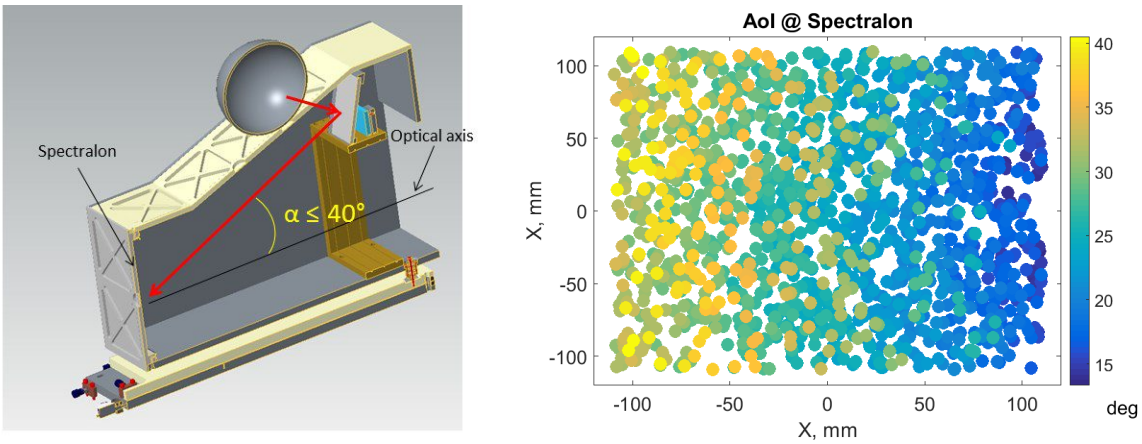

Figure 4, **Left:** The design of the FCU limits the AoI of the rays onto the Spectralon panel at maximum 40° to ensure a quasi-Lambertian diffusion of the light. **Right:** optical simulation of the AoI distribution at the Spectralon panel.

The FCU provides also the absolute wavelength calibration of the MICADO spectrograph by means of four gas lamps (Ar, Kr, Xe, Ne) whose light is also projected onto the Spectralon panel and fed by the standalone RO/ the MAORY optics to the MICADO slit. The selection of light sources used by X-shooter has been adopted as baseline also for MICADO being comparable with respect to both the spectrograph resolution (R~14,000) and the wavelength range [5]. Two optical layouts for the wavelength calibration segment of the FCU are under study in parallel as shown in Figure 5:

- FCU design solution **1**: the gas lamps bypass the IS and their light is conveyed to the Spectralon panel via optical fibres; one scattering process -> Spectralon.

- FCU design solution **2**: the gas lamps are placed inside the IS as the flat-field lamp; two scattering processes, the light is firstly homogenized in the IS and subsequently diffused by the Spectralon panel -> IS + Spectralon.

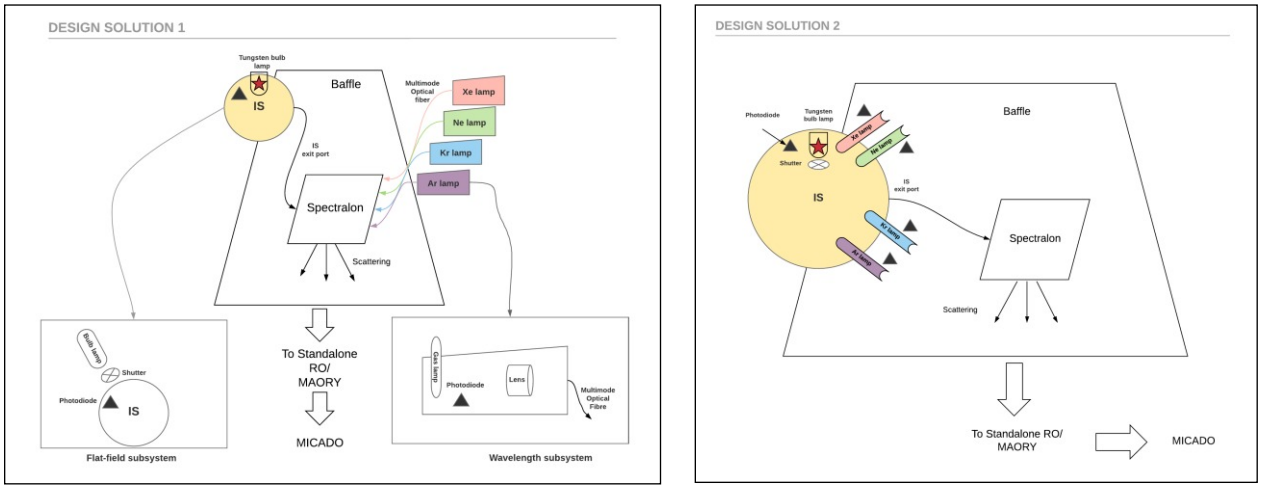

Figure 5, **Left:** design solution 1, the gas lamps bypass the IS and their light is conveyed to the Spectralon panel via optical fibres, the IS is used only for the flat-field calibration. **Right:** the gas lamps are plug into the IS and undergo two scattering processes (lower efficiency).

The IS estimated typical efficiency for a sphere of 280 mm diameter and an exit port of 50 mm is:

$$\eta = \frac{A_{exit\ port}}{A_{exit\ port} + \alpha(A_{IS} - A_{exit\ port})} \approx 13.8\ \%$$

with α = 0.05 typical absorption coefficient of the IS coating. Polychromatic ray tracing simulations with Zemax taking into account the Spectralon spectral reflectance estimate an efficiency of 11.3 %. The scattering process at the Spectralon panel is simulated in Zemax and leads to an estimated overall efficiency of the FCU of $\eta_{IS+Spectralon} \approx$ 9e-5. A design option with better efficiency (solution 1) foresees to place the gas lamps in four separate boxes equipped with a lens collimator that injects the light from a 7 mm fraction of the lamp gas bulb into a multimode fibre (core diameter 1,500 µm), Figure 6. The light coming out of the fibre is projected onto the Spectralon panel bypassing the IS. The coupling of light into the optical fibre efficiency is given by its throughput (~ 13.5%) fully comparable with that of the IS, but when the gas lamps are placed into the IS, there is no control of the beam shape out of it. The benefit of conveying the light with an optical fibre is the possibility of projecting a specific beam footprint onto the Spectralon panel. The numerical aperture (NA) of the optical fibre is NA = 0.22 and by placing the fibre at a specific distance from the Spectralon panel a smaller region of it, corresponding to the spectrograph slit length footprint, can be illuminated without dispersing excessively the light flux.

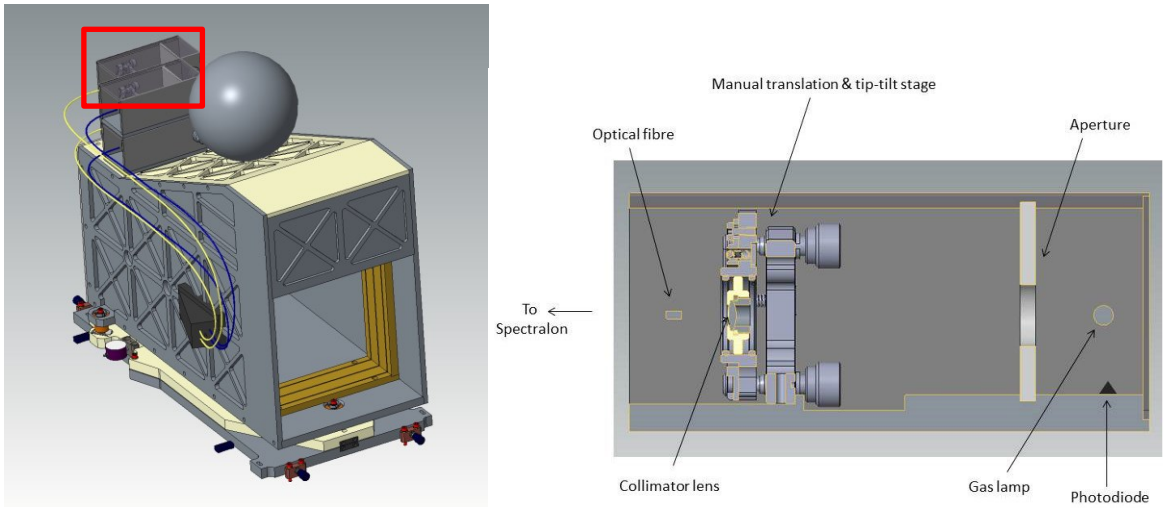

Figure 6: View of the FCU with the gas lamps bypassing the IS with an optical fiber as proposed in design solution 1 (Fig. 5 left). Each gas lamp is placed in a separate box (red highlighted) equipped with a focusing lens to inject the light into the fiber that coveys it to the Spectralon panel (right).

Two spectrograph slits are expected in MICADO, lengths 3" and 15", e.g. ≈ 10 and 50 mm at the instrument entrance focal plane. The overall efficiency of the FCU in this design option is $\eta_{fibre+Spectralon} \approx$ 2.83e-3 that is more than an order of magnitude better than $\eta_{IS+Spectralon} \approx$ 9e-5. The final design solution will be chosen after the PDR based on the outcome of the testing of the prototype FCU under development at MPIA. Fourier Transform Spectrometer (FTS) spectra of the gas lamps have been taken at the Institut für Astrophysik IAG (Fig. 7) to provide an estimation of the number of calibration lines available at the MICADO resolution. The gas lamp spectra are measured with the IFS Bruker 125HR FTS using three different detectors, Si Diode, InGaAs and InSb to cover the spectral range of 0.8 - 2.4 µm. The absolute

flux from the brightest lines has been estimated using a series of NIR filters and a calibrated photodiode to assess the detectability and the Signal to Noise Ratio (SNR) during typical calibration exposures for the two FCU design options.

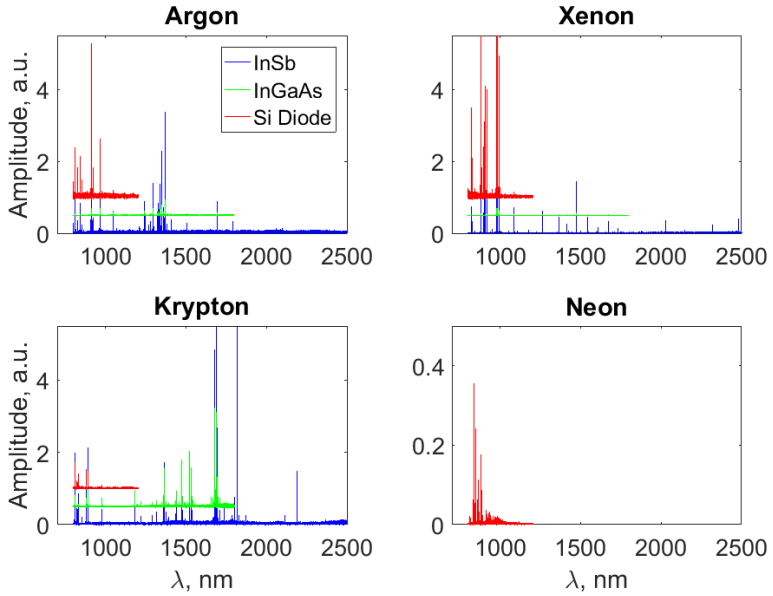

Figure 7: FTS spectra of the gas lamps obtained at IAG with three different detectors in the range 0.8 - 2.4 µm. The Ne spectrum is incomplete due to a combination of technical problems and a noisy spectrum of the lamp of which the causes are under investigation.

Once the FTS spectra will be fully analysed and a full spectrum of the Ne lamp will be available, the MICADO instrument simulator SimCADO [10] shall simulate a typical spectrum with the four gas lamps as seen with the instrument. At the moderate spectral resolution of MICADO a good rule of thumb is having at least ten calibration lines per order [11]. To mitigate the issues given by the segmentation of the MICADO detector focal plane array, the geometry/orientation of the echellogramm on the focal plane, the spectral distribution of the calibration lines along a certain order, and to strengthen the wavelength calibration, one or more Fabry-Pérot units are studied as potential upgrade of the baseline wavelength calibration hardware. For this upgrade option, not in the baseline design of the MCA for PDR, two different solutions are under study: a fiber-fed Fabry-Pérot as adopted by CRIRES+ [12] and single mode fiber Fabry-Perot operated with a supercontinuum laser or a superluminescent diode as in APOGEE [13].

2.3 Astrometric calibration unit - ACU

The ACU is responsible for the calibration of the most delicate and challenging observing mode of MICADO: astrometry. The ACU shall map the optical distortions of all RO resp. MAORY and MICADO optics within the MICADO FoV, the drift of distortions due to thermal and opto-mechanical instabilities in the two instruments, distortion changes due to the relative derotation of MICADO against the standalone RO resp. MAORY, and the distortions arising from the IF tolerances between the standalone RO resp. MAORY instrument and MICADO (e.g. Nasmyth platform motion). The ACU will also allow studying the high order distortions originating from the mid spatial frequency residuals of the instrument optics and the detector intra-pixel sensitivity variation. The key element of the ACU is the Warm Astrometric Mask (WAM) that is a reference target mask delivering diffraction-limited point-like sources to be

re-imaged by the instruments through their optics down to the MICADO focal plane. The position of the WAM's point-like sources (pinholes) and the comparison of the latter with the image spots on the MICADO detector leads to estimate the distortion of the instrument optics. The WAM is a ~ 200 mm x 200 mm x 4 mm substrate of Zerodur (Class I) coated with a chrome layer opaque at VIS and NIR wavelengths. The point-like sources of the WAM are realized by etching the coating layer with a laser to create a series of pinholes transparent to light (0.8 - 2.4 µm). The WAM is backside illuminated with a continuous light from eight miniaturized tungsten bulb lamps MGG 4115-09 (Figure 8). The light is diffused from a Spectralon panel behind the WAM as shown in Fig. 8. The light passing through the WAM pinholes undergoes diffraction and creates a collection of point-like sources with high SNR that feeds densely the instruments FoV creating a set of Airy-disk shaped PSFs. The mask is deployed at the entrance focal plane of the standalone RO resp. the MAORY instrument with the DMU and reimaged by both, the standalone RO resp. the MAORY instrument and MICADO. To assess the feasibility and the reliability of the WAM a prototype, scaled 1:2, has been procured from IMT and it is currently being tested at MPIA (Fig. 8).

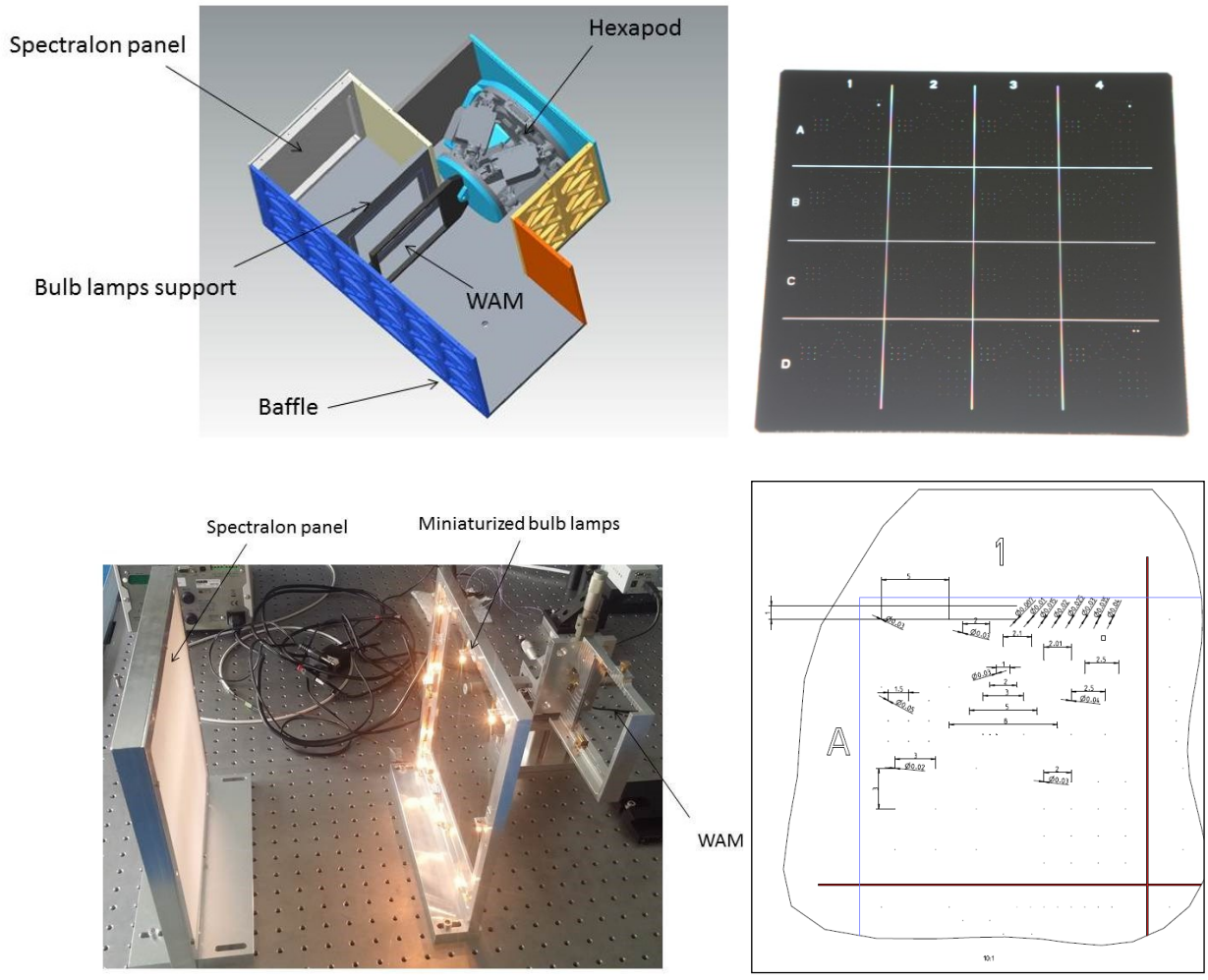

Figure 8, **Top-left:** Insight of the ACU highlighting the hexapod that controls the WAM position, the illumination system based on a series of miniaturized bulb lamps and a Spectralon panel. **Top-bottom-right:** WAM prototype, scaled 1:2, to test different pinhole diameters and the manufacturing position precision. **Bottom-left:** prototype of the ACU with the illumination system.

The duty cycle of the astrometric calibration is difficult to estimate. Ideally the run should take place at every astrometric observation before the beginning of the night and periodically during the night-time; the frequency of the night-time calibration depends on the opto-mechanical stability of the standalone RO/ resp. the MAORY optics, MICADO and their interface. As shown in Figure 8, the WAM is mounted on a hexapod to allow fine-positioning the mask with the maximum DoF. The hexapod allows refocusing the image of the WAM to compensate for differential motions of the MICADO instrument and e.g. MAORY, and to allow the dithering of the mask for an increased spatial sampling of the distortion pattern. More details of the prototypes tests and issues related to the astrometric calibration are discussed in sections 3.1 and 4.

2.4 Movable source calibration unit - MCU

The third MCA subsystem is the movable source calibration unit (MCU) that shall provide a VIS-NIR (0.5 μm to 1.5 μm) continuum, diffraction-limited light source capable of patrolling the SCAO WaveFront Sensor (WFS) FoV (80 mm x 40 mm). The MCU shall be visible both from the SCAO WFS (in VIS wavelength range) and the MICADO detector (in NIR wavelength range) and it shall have a tuneable flux. The light from a halogen lamp is coupled with a multi-mode fiber diffraction-limited that is mounted on a 3-D PI linear stage and a small manual tip-tilt stage to have high flexibility in patrolling the SCAO WFS FoV, and to allow for refocussing and optimizing the alignment of the source (Fig. 9).

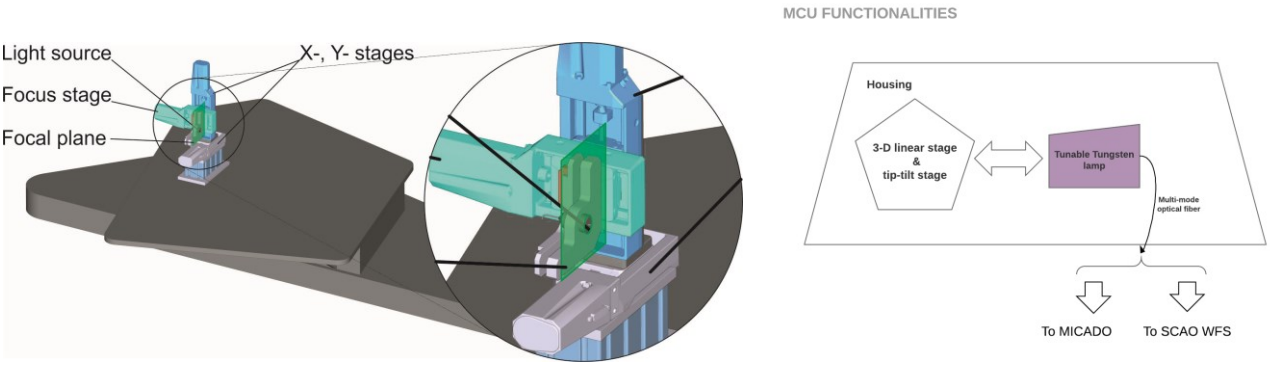

Figure 9: Layout of the MCU mounted on manual tip-tilt stage and a linear motorized 3-D stage assembly. The light source from a halogen lamp is coupled to a multi-mode diffraction-limited optical fiber optimized to transmit between 0.5 μm to 1.5 μm visible for the MICADO detector and the SCAO WFS.

The purpose of the MCU is twofold: providing a movable source to simulate a differential tracking motion onto the SCAO WFS and supporting the integration of the cryostat-detorator in the identification of the rotation axis every time the cryostat is mounted/dismounted from the rest of the instrument. In the first case, the MCU is used to mimic a differential tracking motion within the SCAO WFS FoV and to calibrate the latter for non-sidereal AO observations of e.g. solar system objects. During such observations the SCAO WFS tracks the guide target with the SCAO field selector and the telescope tracks the scientific object. To test the correct functioning of the SCAO field selector, a movable source is required since the AO loop cannot be closed using the science object that is moving differentially with respect to the guide star, while the calculation of the differential trajectory is left to the instrument control software/observer. The second functionality of the MCU is supporting the cryostat-detorator axis identification following a simple day-time

procedure: (i) the MCU source is reimaged with the MICADO camera, (ii) the derotator is rotated by a certain angle, (iii) another image of the MCU is taken and (iv) the light source is moved towards the center of rotation of the derotator until the source image spot does not move anymore, (v) the SCAO WFS position is registered and locked. Differential tracking observations and dismantling/mounting of the cryostat are expected to take place sporadically. Nevertheless the MCU might support also the AIV and commissioning, diagnostic and maintenance operations of MICADO at the telescope.

3. PRELIMINARY RESULTS OF PROTOTYPES TESTING

3.1 WAM prototype assessment test

To support the WAM development and assessing its technology readiness level, a scaled 1:2 prototype has been procured from IMT. The size of the WAM prototype has dimensions 101 mm x 101 mm x 2 mm. It carries 4 x 4 cells of a custom pattern, optimized for the test purposes (see Fig. 8 bottom-right). Each cell contains different pinholes sizes and separations. This prototype will allow selecting the most suitable pinhole diameter in terms of SNR during a calibration frame and it will provide the opportunity of measuring the manufacturing precision of the pinholes placement on the mask. Those aspects are the key parameters for the astrometric calibration of the instrument. Figure 10 shows the results of the measured absolute flux from different WAM pinhole diameters obtained with a calibrated InGaAs photodiode and two quasi J-H band filters realized with long and short pass band filters in combination with the calibrated photodiode responsivity (Fig. 10 right). During the measurement the WAM prototype is back-side illuminated with the same system as designated for the final ACU design as described in section 2.3.

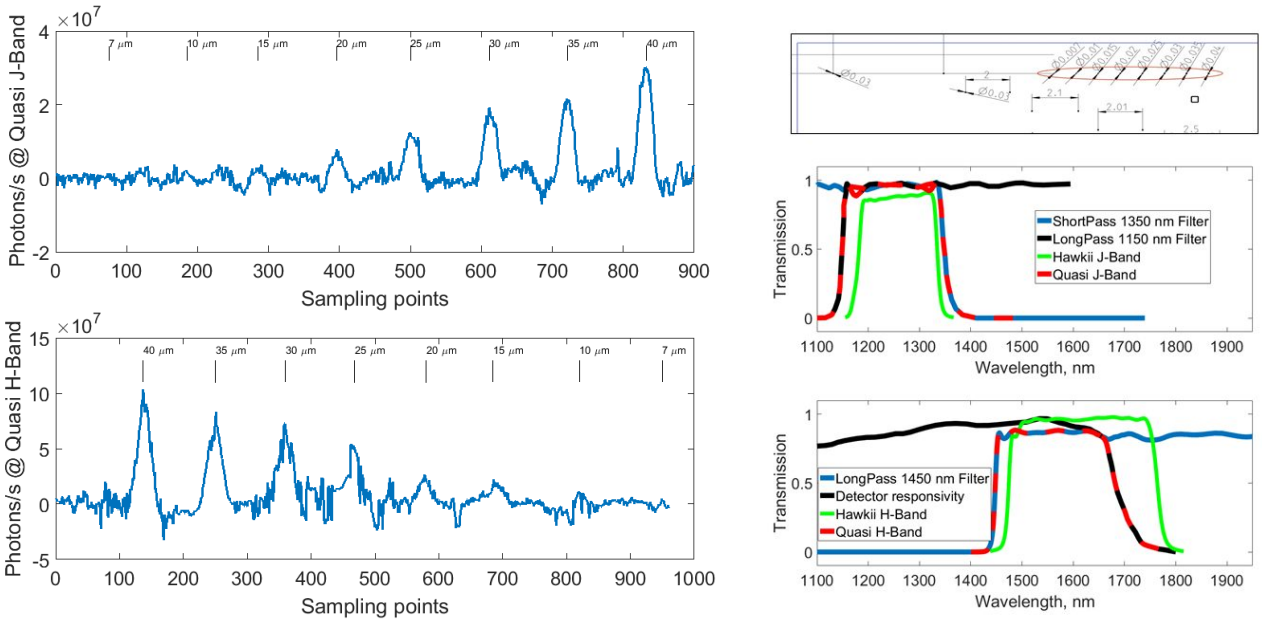

Figure 10, **Left:** Absolute flux measured with a row of pinholes with different diameters 40-35-30-25-20-15-10-7 µm in quasi J-H band filters. The measurement is obtained moving the WAM with a motorized stage in front of the calibrated photodiode. **Right:** Transmission curves of the quasi J-H band filters obtained with long and short pass band filters in combination with the calibrated photodiode responsivity.

Taking into account the internal transmission of standalone the RO resp. the MAORY instrument and MICADO and the size of the instrument PSF, the estimated signal in J-H bands at the instrument focal plane is $S \sim 10^5$-10^6 ph/s/pixel, that ensures a reliable and fast astrometric calibration in all the MICADO filters.

To assess the manufacturing precision of the WAM prototype, more specifically the pinhole positions precision, a test setup based on the so called double slit Young's double slit experiment has been realized at MPIA (Fig. 11): a coherent light source (He-Ne laser) is projected onto a pair of pinholes and the interference pattern is recorded with a CMOS camera at a certain distance from the WAM (~ 300 mm). The pinhole separation d is estimated measuring the fringes separation Δf on the detector and knowing the WAM-to-detector separation z:

$$d = \frac{z\lambda}{\Delta f} \qquad \text{(Eq. 1)}$$

A non-trivial component of the measurement is given by the precise estimation of the WAM-to-detector separation for which a dedicated Michelson interferometer has been set up to track any relative displacement between the two objects. The monitor of the WAM-to-detector (CMOS1) separation changes is achieved by means of the low coherence interferometry (LCI) technique [14] by tracking the displacement of a fringe envelope from a superluminescent low coherence diode (SLED) injected with a single mode fiber into the interferometer (Fig. 11). One arm (ARM1) is carrying the WAM prototype and constitutes the WAM-to-detector baseline to be measured; the other arm is mounted on a carbon fiber bench whose thermal expansion is assumed negligible in comparison with the optical bench: any thermal drift of the bench and any mechanical displacement of the WAM induces a shift of the LCI fringe envelope that is translated in a separation measurement by measuring the fringe centroid with CMOS2 [14]. To measure different pinhole pairs, the WAM is moved with a manual 3-D linear stage. Each WAM pinhole fringe pattern is associated with a certain LCI measurement.

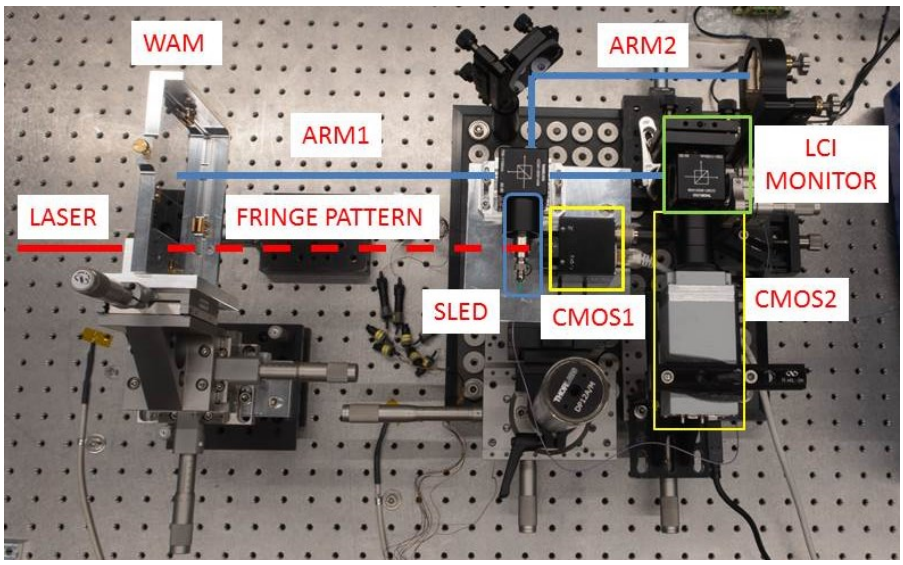

Figure 11: MPIA lab setup for the measurement of the WAM prototype pinholes position. The setup mimics a Young's double slit experiment with the laser illuminating a pair of pinholes on the WAM and a detector collects the fringes to estimate d of Eq. 1. A LCI Michelson interferometer is realized to monitor the separation between the WAM and the detector. In the ARM1 the WAM is used as mirror for the interferometer while ARM2 is assumed to be fixed being mounted on a carbon fiber bench with ultra-low thermal expansion. CMOS 1 is used to record the Young's fringes, while the CMOS2 tracks the SLED fringe shift in the LCI.

The manufacturing company of the WAM prototype gives an expected manufacturing residual error for the pinholes positions onto the mask that scales with the linear size of the mask L:

$$\sigma(\mu m) \sim \pm(0.5\mu m + 5 \times 10^{-6} L(m)) \qquad \text{(Eq. 2)}$$

For the WAM prototype the expected maximum pinhole relative positioning error over the full mask (large-scale) is σ ~ 1 μm, while the local position error between two pinholes 1-2 mm apart (small scale) is expected to be about ~ 10 nm. In the Young's setup each image of the fringe pattern (Fig. 12 top-left) is corrected for flat-field and dark and the image counts are summed into stacked columns to create a 1-D strip. A passband filter is applied to remove the low and high spatial frequencies and to isolate the fundamental harmonic associated with the fringe separation Δf.

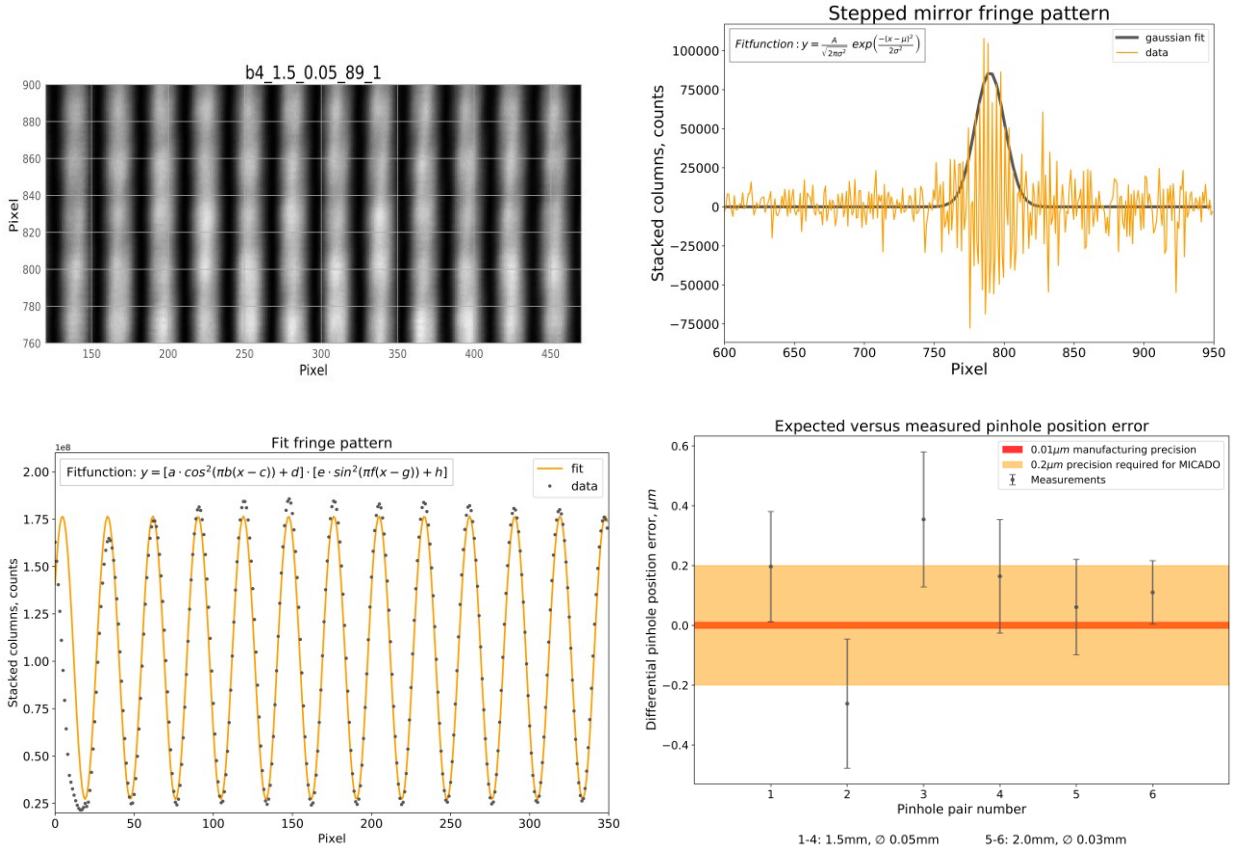

Figure 12, **Top-left:** Fringe pattern from a pair of 50 μm pinholes 1.5 mm apart. **Bottom-left**: Fit of the stacked fringe pattern. **Bottom-right**: estimated pinholes position measured with the setup of Fig. 11; the red strip represents the expected 2 mm-scale manufacturing precision as given in Eq. 2, the orange strip the MICADO astrometric driving requirement of Eq. 3. **Top-right**: fringe pattern from the SLED whose centroid is used to track and measure the separation between the WAM prototype and the detector.

The fringe pattern is fit with the function approximating the Fraunhofer diffraction $\sim cos^2(\Delta f) sin^2(a)$ to find the best fitting Δf value (Fig. 12 bottom-left); the pinholes separation is then estimated using Eq. 1 (a is the pinhole diameter).

To achieve the goal of the MICADO astrometry (50 μas, [2]) the pinhole position should be known with a precision of ~ 200 nm as reported by [15] and estimated below:

$$\delta \mathrm{l}_{\mathrm{pinhole}} = l_{WAM} \times \sigma_{astrometry}/\mathrm{FoV} \sim 0.2\ \mathrm{m} \times 50\text{e-}6"/53" \sim 200\ \mathrm{nm} \qquad \text{(Eq. 3)}$$

The measurement following the Young's technique can effectively provide submicron precision for the pinholes position even though it measures the separation between two pinholes *d* and not directly the pinhole position. The assumption we make is that the estimated manufacturing error Δd is equally divided between the two pinholes. The measurement is feasible only for small pinhole separations, d_{max} = 1-8 mm, beyond, the fringes density becomes a limiting factor in the precision of the measurement. The main drawback of this measurement is the time-consumption of the technique. As shown in section 4, to map the higher order distortions from the instrument optics the WAM pinholes number density has to be about 4-to-9/mm^2, that over a 200 mm x 200 mm mask translates in an impractically large number to be singularly measured. The WAM can be also dithered for the distortion calibration so the number of pinholes can be reduced, but still it will be in the order of a few thousand. The current test baseline consists into an extended testing of the WAM prototype following the above described technique to qualify the production process of such a mask and prove the technology reliability so that a comparable error budget can be assumed also for the final WAM (prior some random pinholes checks). The CMOS1 pixel scale is 4.4 μm/pixel and it has a sensitive area of 7.13 x 5.4 mm. The FWHM of the Young's fringes from two 50 μm pinholes in the current setup is ~ 14 pixels. With typical fringe SNR ~ 5e3, in combination with the large number of fringes per frame ~ 60, allows for fringe spatial frequency estimation at the level of:

$$\delta f = \mathrm{FWHM(f)}/\mathrm{SNR(f)} \times 1/N_{fringe} \times 1/(\Delta \mathrm{f} \times \mathrm{FWHM(f)}) \sim 1\text{e-}6 \qquad \text{(Eq. 4)}$$

That leads to a nominal precision of Δd ~ 10-20 nm over scales of *d* ~ 1-2 mm. The factor limiting the final precision of the test setup is represented by the measurement of the absolute length of the ARM1 baseline that is known with an error of δz ~ 20 μm coming from the calliper measurement and the mechanical manufacturing precision of the supporting plates of the interferometer components. Differential changes and mechanical drifts of the WAM position in ARM1 are measured with the LCI technique at submicron precision, but the systematic δz ~ 20 μm limits the achievable precision of the pinhole position to ~ 100-200 nm (Fig. 12 bottom-right). We conclude that the nominal manufacturing precision (10 nm/2 mm) is sufficient for our needs and it has been successfully probed down to 100-200 nm scales over different WAM sub-regions. After intensive testing at MPIA the WAM prototype will be shipped to ESO Paranal (end of 2018) to be exposed for one year to the environmental conditions expected at Cerro Armazones to assess the impact of dust, sand, aerosol, carbon compounds, oxygen and water vapour on the coating aging process. The WAM will be placed in a protecting box that allows air exchanges with the environment while protecting mechanically the WAM from accidental collisions or fingerprints. The box will be returned to MPIA after a full year of permanence at Paranal for the coating inspection and evaluation.

3.2 MCA light sources selection and assessment test

The light sources of the FCU and the ACU have been tested to assess the short and long term stability and the warming up time. The setup used for the measurements consists of a light-tight barrel that hosts the light source under test, a calibrated InGaAs photodiode, one or more filters and a pinhole/aperture. The calibrated photodiode is equipped with a temperature sensor to track the thermal drifts and its dark current. The spectral calibration gas lamps show a flux (F)

stability of $\Delta F/\Delta t \approx 3\%/h$ (Fig. 13 Top-left). As the flux doesn't vary significantly after switching on the lamps there is no need for a warming up procedure (see also Fig. 13, Top right). The flat-field lamp (model Osram Halostar Starlite 10 W 12 V) shows a good stability and linearity $\Delta F/\Delta t \approx 0.2$ %/h and the need of a 5 minutes warming up time partially due to the thermalization of the lamp housing (Fig. 13 Bottom-left). The ACU lamps require 1 minute of warming up time, afterwards the flux is stable within $\Delta F/\Delta t \approx 0.01\%/0.5$ h. Long-term, intensive, stability tests with operation times typical of the calibration duty cycle show good performance and no significant variations with respect to the trends reported in Fig. 13. The light source not yet tested is the MCU. A possible candidate light source has been selected, but not yet procured and tested.

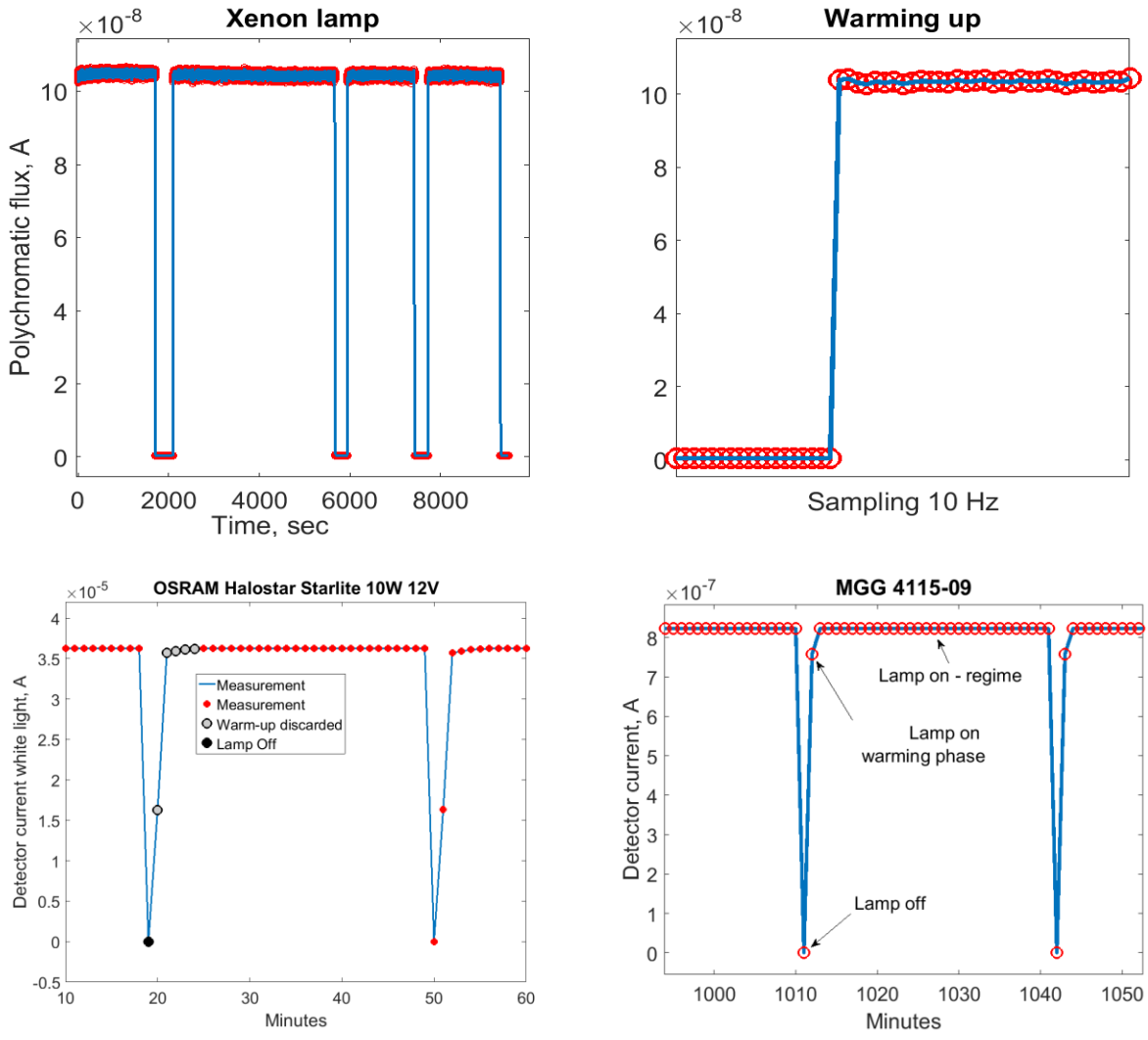

Figure 13, **Top:** polychromatic light flux during on-off cycles of the Xe gas lamp; the lamp does not show any latency during the warming up phase. **Bottom-left**: linearity of the flat-field lamp during typical calibration duty cycles; the lamp requires 5 minutes of warming up time to reach a stable flux. **Bottom-right**: linearity of the MGG 4115-09 ACU lamps during typical calibration duty cycles; the lamp requires 1 minute of warming up time to reach a stable flux.

All the light sources of the FCU and ACU have been successfully tested and they meet the requirements of the MCA. For the FCU alternative light sources will be investigated to shorten the warm-up time.

4. POTENTIALITIES AND LIMITATIONS OF ASTROMETRIC CALIBRATION

In the current design concept, MAORY receives a curved FP from the ELT (R ~ - 9884 ± 70 mm) [16] and it delivers a flat FP to MICADO. The current baseline for the astrometric calibration relies instead on a flat WAM that is significantly easier to manufacture and test. This curvature mismatch leads to two problems:

- It introduces a progressive defocus of the PSFs in MICADO proportional to their position in the FP: the centre of the FP is barely sensitive while the corners suffer increasing defocus and Strehl ratio deterioration (~ 0.8 SR).

- It creates a projection effect from a spherical surface to a plane, this has a direct impact on the astrometric position of the pinholes in the image plane: the FP is radially stretched as a result of an orthographic projection [17] as shown in Figure 14.

The magnitude of the defocus can be efficiently controlled by repositioning the WAM axially by a fraction of mm using its hexapod (Fig. 15 left). The distortion introduced by the orthographic projection cannot be avoided. As shown in Figure 14, this projection causes a systematic shift of the centroids of the WAM image spots that has a maximum at the edge of the FoV (~ 0.8 mas). The introduced distortion pattern is however very regular and it can be described by a plate scale term. The curvature mismatch leads also to a slightly different optical path within the instrument between the astrometric calibration light and the starlight. Taking a closer look onto the last reflecting surface of MICADO that is part of the three mirror anastigmat camera (TMA), the footprint of the light beams at this surface is shifted by ~ 4.5 µm (Fig. 15 right).

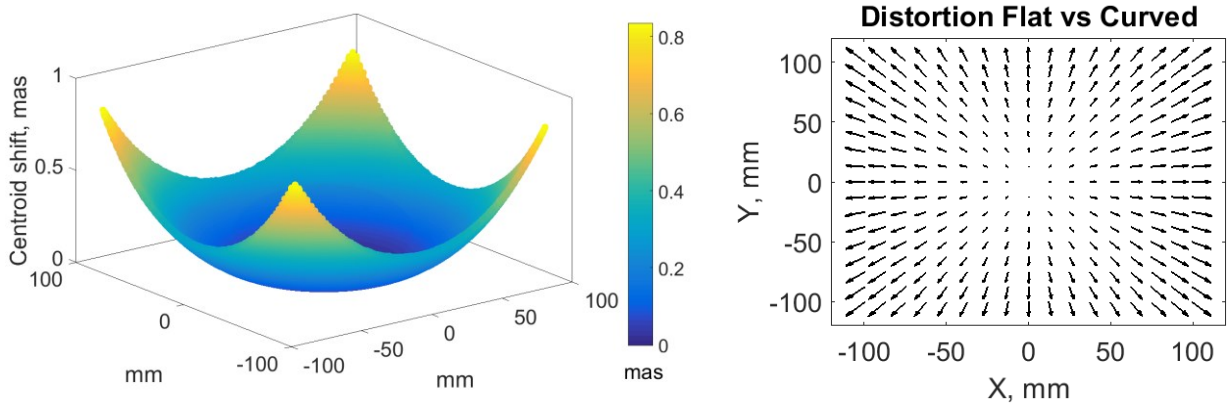

Figure 14, **Left:** Centroid shift induced by using a flat WAM at the entrance focal plane of the instrument designed for a wavefront curvature of ~ -9884 mm. **Right**: Geometric distortion induced by a flat WAM deployed at the instrument entrance focal plane, the distortion can be described by a plate scale term.

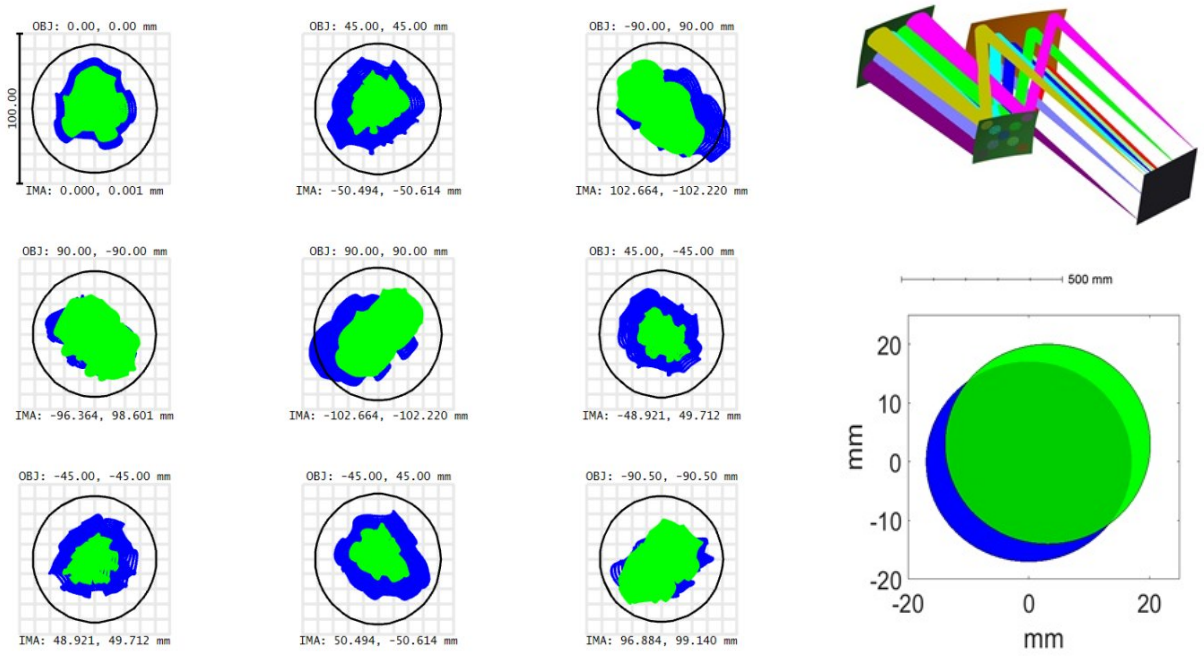

Figure 15, **Left:** MICADO PSFs at different field points in the presence of mid-spatial frequencies errors (MSFEs) on the last TMA surface for the nominal curved ELT input FP (blue) and the flat FP, equivalent to the WAM (green). The PSFs rims are irregular due to the MSFEs, but despite the latter and the curvature mismatch, the overall PSF sizes remain within the diffraction limit of the instrument (black circles). **Right-top:** Beam footprint of different fields at the last reflecting TMA surface (orange). **Right-bottom**: Magnified view of the offset (x1000) between the nominal beam footprint (blue) and that from a flat WAM (green) at the last TMA surface; the size of the beam is about 34 mm in diameter and the offset induced by the use of a flat WAM is in the order of ~ 4.5 µm.

The optical surfaces close to the FP are particularly important for the control of the distortions production within the instrument given their high optical leverage from the combination of the converging beam towards the FP and unavoidable presence of mid-spatial frequencies errors (MSFE) residuals of the manufacturing process [18]. The MSFE pattern depends on the manufacturing technology: for the TMA production we expect residuals features at a spatial scale of 5 mm that is the approximate size of the manufacturing tool. In Figure 16 (left) we report three simulated MSFE patterns for the last reflecting surface of the TMA and the corresponding distortion pattern (right) over a MICADO FP region of 3.3 arcsec^2 (10 mm^2). The first pattern is characterized by a random white noise pattern with a peak to valley (PV) of 20 nm, the middle pattern includes in addition vertical and horizontal strips and the bottom the surface has a white noise pattern plus the first 15 Zernike terms in Noll notation [19] as residual manufacturing errors.

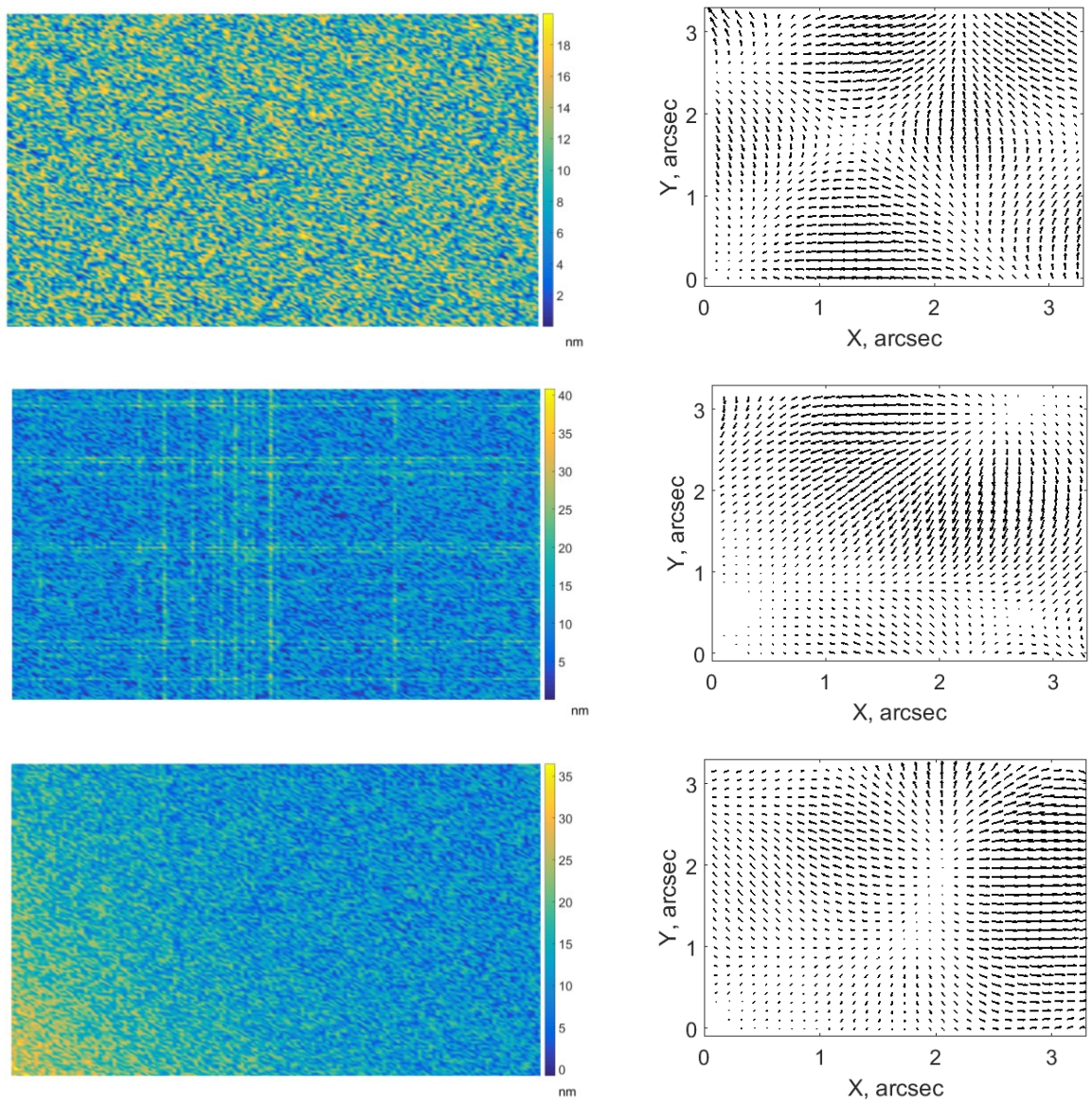

Figure 16, **Top:** Simulated manufacturing residuals mid spatial frequency errors (MSFE) expected for a mirror machining tool of 5 mm with a white noise spectrum and a PV ≈ 20 nm at the last TMA surface. On the **right**, the corresponding distortion map over 3 arcsec^2 at the MICADO focal plane. **Middle:** Simulated manufacturing residuals MSFEs for a white noise spectrum and vertical and horizontal strips and corresponding distortion map over 3 arcsec^2. **Bottom:** White noise + the first 15 Zernike polynomials and corresponding distortion map over 3 arcsec^2.

The spatial sampling of the distortion pattern shown in Fig. 16 is equivalent to deploy a WAM with a pinhole pitch of 0.33 mm. The distortion pattern is fitted with a series of increasing order polynomials with a Cartesian basis [20] and the residual root mean square (RMS) are plotted in Fig. 17 (right) for both cases of a flat and a curved WAM. Using a flat WAM versus a curved solution seems not to decrease the astrometric precision of MICADO. The RMS distortion drops below the MICADO astrometric requirement (50 μas) for polynomial orders equal and greater to 7th. The high order polynomials require a large number of sampling points whose availability is ensured by the WAM pinholes grid. The power spectra of the simulated MSFE patterns are shown in Fig. 17 (left).

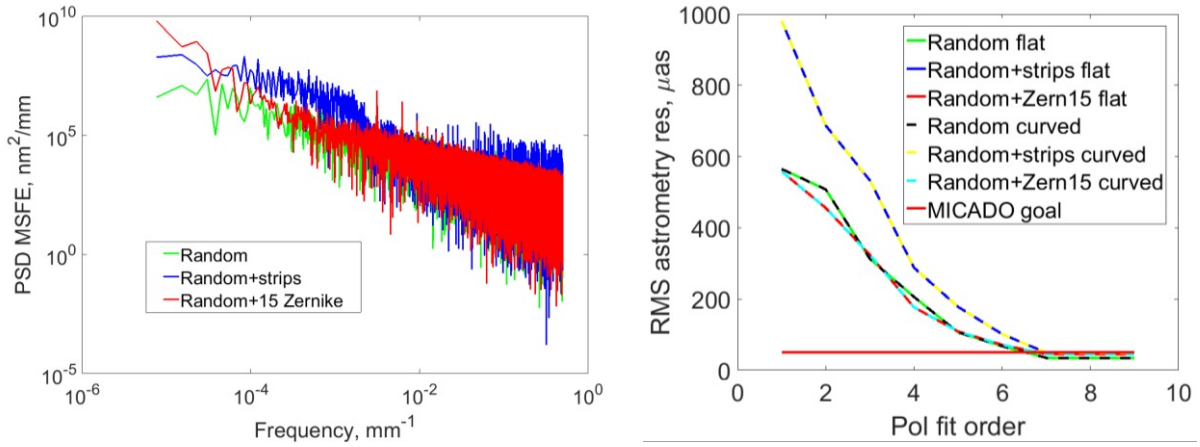

Figure 17, **Left:** Power spectra of the simulated residuals MSFE expected for a mirror machining tool of 5 mm. **Right:** The rms astrometric residual subsequently to polynomial fits of increasing orders. The rms astrometric residual error is smaller than the MICADO requirement for polynomial orders $\geq 7^{th}$.

In conclusion we underline that the WAM can calibrate the instrument distortion of the standalone RO resp. the MAORY instrument and MICADO, but it cannot control the distortions from the telescope. The calibration of the latter has to be done on sky using reference stars field from the GAIA catalogue and/or a self-calibration on the science target field. A description of the techniques and of the telescope contribution to the MICADO error budget can be found in [21].

5. CONCLUSIONS

The presented work describes the preliminary design of the MICADO calibration assembly to fulfil flat-field, wavelength and astrometric calibration and supporting the instrument alignment to the SCAO wavefront sensor. The on-going prototype test campaign has led to identify suitable light sources for the FCU and ACU subsystems and to verify the manufacturing precision of the WAM. The design and prototyping work is constantly supported by the simulation counterpart to assess the impact of a certain design concept or technology limitation. The current design concept will be presented as baseline for the MICADO PDR.

ACKNOWLEDGEMENTS

Authors are warmly grateful to Dr. Florian Kerber for the discussion and inputs for the FCU and ACU development; to Armin Boehm, Luigi Lessio for the prototype test setup, and to Vincenzo De Caprio, Fausto Cortecchia, Emiliano Diolaiti and Paolo Ciliegi for the discussion about the MCA deployment strategy on the MAORY bench.

REFERENCES

[1] Diolaiti, E., et al., “Preparing for the phase B of the E-ELT MCAO module project”, Proc. of SPIE Vol. 9148 91480Y-1 (2014).

[2] Davies, R., et al., “MICADO: first light imager for the E-ELT”, Proc. SPIE 9908, Ground-based and Airborne Instrumentation for Astronomy VI, 99081Z.

[3] Neichel, B., Lu, J.R., Rigaut, F., Ammons, M.S., Carrasco, E.R. and Lassalle, E., “Astrometric performance of the Gemini multiconjugate adaptive optics system in crowded fields”, MNRAS 445, 500-514 (2014).

[4] Ciliegi, P., Diolaiti, E., et al., "MAORY for ELT: preliminary design overview", Proc. SPIE, Ground-based and Airborne Instrumentation for Astronomy, 2018.

[5] Vernet, J., et al., “X-shooter, the new wide band intermediate resolution spectrograph at the ESO Very Large Telescope”, A&A 536, A105 (2011).

[6] Kelz, A., Bauer, S.M., Hahn, T., Jahn, T., Kosmalski, J., Laurent, F., Laux, U., Larrieu, M., Loupias M., Olaya, J.C., Popow E., Roth, M. M., Srivastava, M., Streicher O., Weilbacher P. and Bacon, R., “Development and performance of the MUSE calibration unit”, Proc. of SPIE Vol. 8446 84465T-1 (2012).

[7] Lenzen, R., et al., ‘CONICA: The high resolution near-infrared camera for the ESO VLT’, SPIE Vol. 3354 • 0277-786X/981, 1998.

[8] Ramsay, S. K., Rolt, S., Sharples, R. M., and Davies, R., “Calibration of the KMOS multi-field imaging spectrometer”, Proc. 2007 ESO Instrument Calibration Workshop, 319-324 (2008).

[9] Bhandari, A. et al., “Bidirectional reflectance distribution function of Spectralon white reflectance standard illuminated by incoherent unpolarized and plane-polarized light”, Applied Optics, Vol. 50, No. 16, 2011.

[10] Leschinski, K., O. Czoske, R. Köhler, M. Mach, W. Zeilinger, G. Verdoes Kleijn, J. Alves, W. Kausch, N. Przybilla, "SimCADO: an instrument data simulator package for MICADO at the E-ELT", Proc. SPIE 9911, Modeling, Systems Engineering, and Project Management for Astronomy VI, 991124 (8 August 2016); doi: 10.1117/12.2232483.

[11] Florian Kerber, Francesco Saitta, Paul Bristow, Joel Vernet, "Wavelength calibration sources for the near infrared arm of X-shooter", Proc. SPIE 7014, Ground-based and Airborne Instrumentation for Astronomy II, 70143Y (11 July 2008); doi: 10.1117/12.787299.

[12] U. Seemann, G. Anglada-Escude, D. Baade, P. Bristow, R. J. Dorn, R. Follert, D. Gojak, J. Grunhut, A. P. Hatzes, U. Heiter, D. J. Ives, P. Jeep, Y. Jung, H.-U. Käufl, F. Kerber, B. Klein, J.-L. Lizon, M. Lockhart, T. Löwinger, T. Marquart, E. Oliva, J. Paufique, N. Piskunov, Eszter Pozna, A. Reiners, A. Smette, J. Smoker, E. Stempels, E. Valenti, "Wavelength calibration from 1-5µm for the CRIRES+ high-resolution spectrograph at the VLT", Proc. SPIE 9147, Ground-based and Airborne Instrumentation for Astronomy V, 91475G (6 August 2014); doi: 10.1117/12.2056668.

[13] Halverson, Samuel, et al. “Development of Fiber Fabry-Perot Interferometers as Stable Near-Infrared Calibration Sources for High Resolution Spectrographs.” Publications of the Astronomical Society of the Pacific, vol. 126, no. 939, 2014, pp. 445–458. JSTOR, JSTOR, www.jstor.org/stable/10.1086/676649.

[14] Pernechele, C., Fantinel, D., Magrin, D., Lessio, L. and Rodeghiero, G., “Low coherence interferometry-based-meter-distance range finder”, June 2017, DOI: 10.1109/MetroAeroSpace.2017.7999551.

[15] Trippe, S., et al., “High-precision astrometry with MICADO at the European Extremely Large Telescope”, Monthly Notices of the Royal Astronomical Society, Volume 402, Issue 2, 21 February 2010, Pages 1126–1140, https://doi.org/10.1111/j.1365-2966.2009.15940.x

[16] Schmid, C., " Common ICD between the E-ELT Nasmyth Instruments and the Rest of the E-ELT System”, Doc. Number: ESO-264642, 2017-11-07.

[17] Snyder, J. P., Map Projections – A Working Manual, Nov. 12 1987.

[18] Sebastian Scheiding, Christoph Damm, Wolfgang Holota, Thomas Peschel, Andreas Gebhardt, Stefan Risse, Andreas Tünnermann, "Ultra-precisely manufactured mirror assemblies with well-defined reference structures", Proc. SPIE 7739, Modern Technologies in Space- and Ground-based Telescopes and Instrumentation, 773908 (19 July 2010); doi: 10.1117/12.856244; https://doi.org/10.1117/12.856244.

[19] Noll, R.J., “Zernike polynomials and atmospheric turbulence”, J. Opt. Soc. Am., Vol. 66, No. 3 (1976).

[20] Kozhurina-Platais, V., Hammer, D., Dencheva, N. and Hack, W., “Astrometric correction for WFC3/UVIS lithographic-mask pattern”, Instrument Science Report WFC 2013-14.

[21] Rodeghiero G., J.-U. Pott, C. Arcidiacono, D. Massari, M. Glueck, H. Riechert, E. Gendron, “The impact of ELT distortions and instabilities on future astrometric observations”, MNRAS 2018, https://doi.org/10.1093/mnras/sty1426.